CRYSTAL GROWTH & DESIGN

pubs.acs.org/crystal

Article

Thermodynamic and Kinetic Effects on the Nucleation and Growth of ε/κ- or β-Ga_2O_3 by Metal–Organic Vapor Phase Epitaxy

Matteo Bosi,* Luca Seravalli,* Piero Mazzolini, Francesco Mezzadri, and Roberto Fornari

Cite This: *Cryst. Growth Des.* 2021, 21, 6393–6401

Read Online

ACCESS | Metrics & More | Article Recommendations | Supporting Information

ABSTRACT: In this paper, we focus on the growth of β- and ε/κ-Ga_2O_3 thin films via metal–organic vapor phase epitaxy on c-plane sapphire using water and trimethyl-gallium at temperatures between 610 and 650 °C. Using these precursors, the monoclinic β-phase is usually obtained only at temperatures higher than 700 °C. We show here, for the first time, that both β- and ε-Ga_2O_3 can also be obtained by tuning the growth rate of the film, that is, by controlling the supersaturation of the vapor phase. The experimental findings are discussed in the framework of classical nucleation theory and Ostwald's step rule, showing the interplay of thermodynamic (related to different chemical potentials for the metastable ε/κ phase and the stable β phase) and kinetic effects (mainly related to different surface energy barriers for nuclei of different crystallographic phases/planes). The experimental conditions that permit the nucleation and growth of the desired Ga_2O_3 polymorph are identified and thoroughly explained, giving to this work a fundamental as well as a technological relevance.

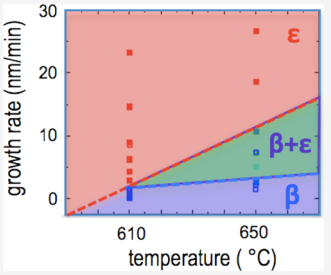

INTRODUCTION

Among wide band gap semiconductors, gallium oxide (Ga_2O_3) is attracting considerable interest for high power electronics and for UVC solar-blind detectors.[1−3]

Ga_2O_3 can exist in different polymorphs, identified as α, β, γ, δ, ε (also referred to as κ), with β-Ga_2O_3 being the thermodynamically stable one.[4] Due to the possibility of growing it from melt and as an epitaxial layer, the monoclinic β-Ga_2O_3 is by far the most studied and technologically mature polymorph, with many device prototypes already produced.[5,6]

Nonetheless, a wide interest is also recently building up on the other polymorphs of this material.[7,8] Apart from a higher symmetry crystal structure with respect to the monoclinic one, which makes them preferable for heteroepitaxial growth and poses fewer problems in film processing and device manufacturing, metastable Ga_2O_3 polymorphs possess unique physical properties that could be particularly advantageous for device engineering. For example, the orthorhombic ε/κ phase has a peculiar spontaneous polarization,[9] which could be advantageous for the realization of heterostructures with high mobility 2D electron gases,[10] while the α phase is characterized by the highest band gap (5.3 eV).[11] The nomenclature of the orthorhombic phase—that is, referred to as ε or κ by different research groups—is still confusing in the Ga_2O_3 community. Due to the presence of 120° rotated orthorhombic domains, resulting in a misleading "pseudo-hexagonal" structure, this polymorph was originally classified as hexagonal ε, but has been later unambiguously identified as purely orthorhombic κ.[12] Nonetheless, the original ε nomenclature of the orthorhombic polymorph is still the most employed one in the vast Ga_2O_3 literature, and it was adopted also in this article.

The growth of ε- or α-Ga_2O_3 is nowadays well established by metal organic vapor phase epitaxy (MOVPE), halide vapor phase epitaxy, mist-chemical vapor deposition (mist-CVD), molecular beam epitaxy, and pulsed laser deposition, and many studies have been devoted to the determination of suitable growth parameters for the stabilization of the desired phase.[7,13] However, besides the experimental aspects of the process and its optimization, in order to get a deeper understanding of the material and improve its development, it is important to comprehend the physical and chemical reasons that rule the nucleation, stabilization, and growth of metastable polymorphs over the stable β phase.

Generally, the nucleation of a metastable polymorph is tightly bonded to both the thermodynamics and the kinetics of the material synthesis, which in turn are strongly dependent on the chosen growth technique. In a recent review paper on Ga_2O_3 thin film growth,[7] some of the authors of this work have already proposed experimental guidelines for the growth of the three most widely investigated polymorphs (i.e., β, α, and ε) with both CVD and physical vapor deposition techniques. It has been shown that (i) chemistry (e.g., metal/oxygen ratio, addition of surfactants, or catalysts during growth), (ii) growth temperature, (iii) type of substrate, and (iv) growth rate (GR) may all contribute to the nucleation and stabilization of a specific polymorph.

In this paper, we focus on the MOVPE growth of Ga_2O_3, a very popular epitaxial method for both basic research and mass

Received: July 30, 2021
Revised: October 4, 2021
Published: October 15, 2021

production of devices. A literature survey reveals that the choice of the chemical precursors can influence the Ga_2O_3 phase stabilization: in the temperature range 600−650 °C, the use of O_2 and trimethyl-gallium (TMG) results in β-Ga_2O_3, while ε-Ga_2O_3 is obtained using H_2O and TMG in the same temperature range. On the other hand, β-Ga_2O_3 was also deposited with H_2O and TMG, but at temperatures higher than 700 °C,[14−16] with the only exception of one work reporting a mixed ε- and β-Ga_2O_3 phase layer at 650 °C,[17] where authors attributed the coexistence of these two polymorphs to their similar free energy and to the lattice mismatch with the hexagonal c-plane sapphire substrate. By decreasing the H_2O flow from 500 to 350 sccm, the ε-Ga_2O_3 phase became dominant. Zhuo et al.[18] grew Ga_2O_3 with O_2 and triethyl-gallium (TEG) with H_2O/TEG ratio between 500 and 1800 and obtained β-Ga_2O_3 for a substrate temperature higher than 510 °C, and the coexistence of β and ε-Ga_2O_3 at lower growth temperatures (500−480 °C) was observed. Pure ε and β- Ga_2O_3 layers were obtained at 500 °C by controlling the MOVPE growth chamber pressure between 3 and 200 mbar using O_2 and TEG as reagents.[19] At low pressure (<20 mbar), a mixed ε/β phase was obtained, while pure ε-Ga_2O_3 was nucleated between 35 and 100 mbar. At higher pressure, β-Ga_2O_3 nuclei formed in the gas phase and nucleated on the substrate surface as a polycrystalline film. A comprehensive overview of the growth conditions for the different polymorphs using various techniques is given in ref 7.

As expected, precursor combination (H_2O or O_2; TMG or TEG), growth temperature, total pressure, and precursor flows (i.e., partial pressures) determine the nucleation of a certain polymorph and its subsequent growth. However, these synthesis parameters are cross-linked among each other, and consequently, the effect on the variation of a single one of them during the MOVPE process (e.g. pressure, temperature, or flow rate) cannot be easily predicted. For example, a temperature variation implies a change of thermodynamic conditions, chemical reaction kinetics, and mobility of adsorbed species at the same time. For this reason, phenomenological observations on the nucleation of a particular polymorph are not sufficient to understand the fundamental factors that affect its stabilization. The macroscopic parameters mentioned above ultimately determine the system supersaturation, that is, the distance of the growth system from the crystal vapor equilibrium conditions, as well as the surface kinetics, and are thus the drivers for the nucleation of a certain polymorph.

In this work, we report on the MOVPE deposition of gallium oxide on c-plane sapphire using TMG and H_2O, and we demonstrate that the growth far from the thermodynamic equilibrium results in metastable ε, while at low or moderate supersaturation, phase-pure β films can be obtained even at temperatures as low as 610 °C.

Understanding the physical reasons behind the nucleation of different Ga_2O_3 polymorphs represents a fundamental step toward tailored material synthesis, and it may provide general guidelines for other deposition techniques.

EXPERIMENTAL SECTION

The epitaxial structures investigated in this work were deposited by MOVPE using TMG and ultrapure H_2O as precursors. TMG and H_2O were stored in stainless steel bubblers kept at 1 and 30 °C, respectively. Helium was used as carrier gas, with a total flow of 400 sccm. Figure 1a shows the horizontal MOVPE reactor chamber used

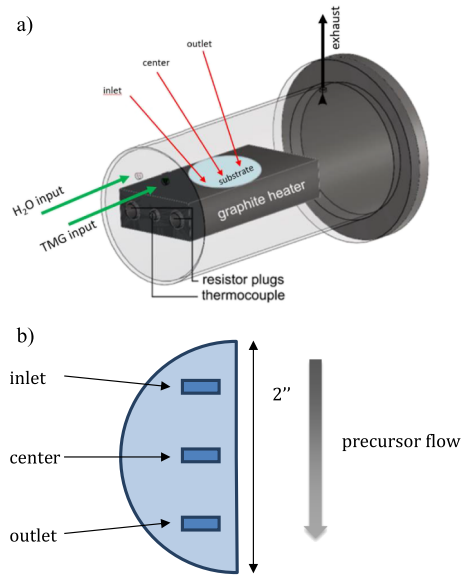

Figure 1. (a) Schematic view of the MOVPE reactor with indication of the investigated zones of the substrate. (b) Top view of half 2″ round sapphire substrate, where the depositions were performed: the rectangles indicate the inlet, center, and outlet zones, where reflectance and X-ray diffraction (XRD) measurements were performed.

in this work, which accommodates a nonrotating graphite substrate holder heated by resistive cartridges. Precursors were delivered in the chamber by two separate gas lines, entering at one end of the chamber at about 15 mm from the substrate. The films were deposited for 150 min at 60 mbar (6000 Pa) on half 2″ c-oriented sapphire substrates (Figure 1b) at temperatures of 650 and 610 °C.

Optical reflectance in the 400−1100 nm range was performed in different zones of the sample using a Jasco UV−vis V-530 spectrophotometer to measure the film thickness and hence calculate the growth rate, considering a refractive index obtained by ellipsometry given by $n(\lambda) = 0.6585 \exp(-2.759 \times 10^{-3}\lambda) + 1.75 \exp(9.837 \times 10^{-5}\lambda)$, where λ is the wavelength in nm (Dr. Peter Petrik, MFA Budapest, Hungary—private communication). The thickness value obtained by reflectivity was validated by cross-sectional scanning electron microscopy (SEM—Zeiss Auriga Compact) (see Figures S1−S4). We estimate that the thickness measured by reflectivity is subject to a 10% uncertainty.

Powder X-rays diffraction data were collected using a Rigaku Smartlab XE diffractometer. 5° Soller slits were placed on both the incident and diffracted beam, and a HyPix3000 2D detector was operated in continuous 1D mode. Measurements were carried out in Bragg−Brentano configuration, making use of CuK_α wavelength, and the K_β component was eliminated by a Ni filter on the diffracted beam. Consequently, all the peaks include the $CuK_{\alpha1}$ and $CuK_{\alpha2}$ contributions, giving rise to a shoulder with $I_{K\alpha1}/I_{K\alpha2} \approx 2$. The incident beam was shaped by fixed divergence slits with 0.1° aperture and by a 2 mm length limiting slit. In such a way, the beam size on the sample is θ-dependent, with 3×2 mm^2 at $2\theta \approx 19°$ and 1×2 mm^2 at $2\theta \approx 60°$. The sample was placed manually in position for each measurement to check the composition at the inlet, center, and outlet zones. Data were collected in the 10−110° 2θ range with 0.01° step size and 10°/min speed.

Quantification of the phases was carried out by Rietveld refinement using the GSAS II suite.[20] 100% preferential orientation was introduced to account for the presence of the sole $(\bar{2}01)$ and (001) families of reflections for the epitaxial β and ε phases, respectively.

https://doi.org/10.1021/acs.cgd.1c00863
Cryst. Growth Des. 2021, 21, 6393−6401

Table 1. Growth Parameters for the Samples Studied in This Work[a]

					inlet	center	outlet	inlet	center	outlet
sample	growth T (°C)	H_2O/TMG	TMG flow	H_2O flow	growth rate (nm/min)			β-Ga_2O_3 fraction (%)		
A	650	200	F_{TMG}	F_{H2O}	26.7	18.7	10.7	1.22	8.1	79.6
B	650	200	1/5 F_{TMG}	1/5 F_{H2O}	7.3	5.1	2.7	43.4	63.8	85.9
C	650	1000	1/5 F_{TMG}	F_{H2O}	6.7	2.8	1.7	95.5	100	100
D	610	200	F_{TMG}	F_{H2O}	23.3	14.7	9	0	0	0
E	610	200	1/5 F_{TMG}	1/5 F_{H2O}	6.3	4.4	3	0.7	2.8	10.6
F	610	1000	1/5 F_{TMG}	F_{H2O}	7.9	4.3	2.8	0	0	82.1
G	610	3800	1/18 F_{TMG}	F_{H2O}	1.3	0.6	0.1–0.2 (islands)	100	100	100

[a]The GR and percentage of β-Ga_2O_3 as obtained by thickness measurements and XRD analysis in the inlet, center, and outlet zone are also reported. The remaining percentage is ε-Ga_2O_3.

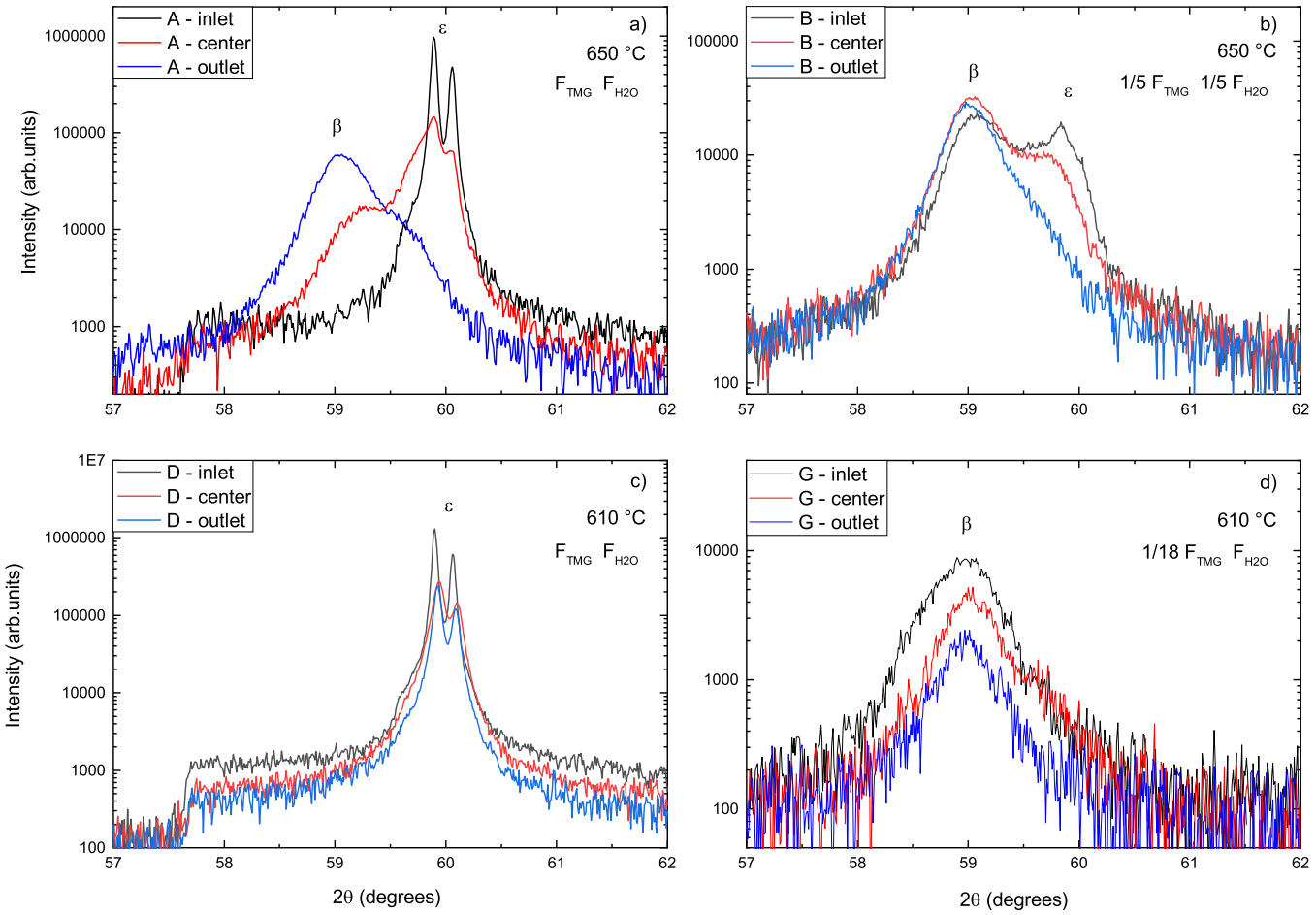

Figure 2. XRD diffraction patterns for the selected samples grown in different conditions: (a) 650 °C in standard flow regime (F_{TMG} and F_{H2O}), (b) 650 °C with a reduced growth rate (1/5 F_{TMG} and 1/5 F_{H2O}), (c) 610 °C in standard flow regime (F_{TMG} and F_{H2O}), and (d) 610 °C with reduced TMG flow (1/18 F_{TMG} and F_{H2O}). The double peaks on the ε phase in (a) and (c) are related to the presence of $CuK_{\alpha 1}$ and $CuK_{\alpha 2}$ wavelengths. The sudden drop at about 57.5° observed in (c) is due to the Ni filter cut.

RESULTS AND DISCUSSION

All the films deposited in these experiments—single or mixed phase—preserve the epitaxial relationship with the substrate and are (001)- and ($\bar{2}$01)-oriented for the ε and β phase, respectively (see Figure S5). The epilayers exhibit a thickness gradient along the flow direction, as the portion of film close to the gas inlet is thicker than the one closer to the reactor exhaust (see Figure 1). Flow dynamics simulations using COMSOL Multiphysics (see the Reactor model paragraph in Supporting Information) suggest that for our typical growth conditions, the gas boundary layer thickness is homogeneous along the flow direction on the susceptor. It is realistic to think of a depletion of precursors along the flow direction, as the growth itself consumes the reagents: different areas of the substrate are thus exposed to different partial pressures of precursors, resulting in a thickness gradient. Given the homogeneous thickness of the boundary layer, we could infer that the growth rate is higher at the reactor inlet, where the precursor concentration in the bulk of the gas phase is higher and so is the diffusion of chemical species toward the substrate. This is a direct consequence of Fick's law, which states that the diffusion of precursors is proportional to the

https://doi.org/10.1021/acs.cgd.1c00863
Cryst. Growth Des. 2021, 21, 6393–6401

concentration gradient of the species. The highest growth rate is obtained in the area closer to the gas input ("inlet", see Figure 1b), while the lowest one is obtained toward the exhaust end ("outlet"). As determined through a first series of depositions made to optimize the process, the growth rate is essentially limited by the TMG flow as the H_2O flow is largely in excess.

The technical design of the growth chamber allows having a homogeneous temperature on the whole substrate surface. Results of COMSOL Multiphysics modeling (see the Reactor model paragraph in Supporting Information),[21] confirmed by direct measurements carried out by placing thermocouples at different points of the heater, indicate that the substrate holder temperature does not deviate from the setpoint by more than +/−5 °C over the entire 2″ pocket that holds the substrate.

These Ga_2O_3 epilayers with variable thickness were considered ideal for an investigation of the relationship between the growth rate (controlled by system thermodynamics and kinetics) and nucleation and stabilization of a certain Ga_2O_3 polymorph. In epitaxy, after having overcome a 2D nucleation threshold typical of any crystallographic plane, the growth rate is directly proportional to supersaturation. Therefore, in the following discussion, we shall assume the growth rate as a measure of supersaturation and we will take it as a suitable parameter to account for the formation of different phases.

Table 1 summarizes the details of all the samples investigated in this study, with indication of the growth conditions, growth rate, and fraction of β polymorph as obtained by XRD analysis in different zones of the layer.

To study the influence of the GR on the Ga_2O_3 polymorph stabilization, we initially defined a standard growth regime in which the precursor flows resulted in a partial pressure of about 6.6×10^{-4} and 1.35×10^{-1} for TMG and H_2O, respectively. The "standard" flows (indicated as F_{TMG} and F_{H2O} in Table 1) are the result of our optimized growth process, which helps obtain good quality single-phase ε-Ga_2O_3 films.[14,22] In the course of the work, we explored the following for both 610 and 650 °C growth temperatures:

- A lower GR regime in which both precursors flows were decreased to 1/5 of their original values (1/5 F_{TMG} and 1/5 F_{H2O}), while maintaining the standard flow ratio;
- The effect of gas stoichiometry variation by changing only the TMG flow, which was reduced to 1/5 of its original value (1/5 F_{TMG}), keeping the H_2O flow at its standard value;
- A TMG flow reduction to 1/18 of its original value (1/18 F_{TMG}), while the H_2O flow was kept at its standard value.

By observing that samples grown in standard conditions at 610 and 650 °C (A and D) have a similar GR, it is possible to state that our deposition rate is mainly limited by mass transport. However, the slight difference in the GR at the two temperatures may suggest that kinetics is still playing a role, and the process occurs in the transition region between the kinetic-controlled regime and the mass transport one (although shifted toward the latter). The growths exhibited at the same temperature but with different flows (A vs B and D vs E) also indicate mass transport as the decisive factor for the GR.

By using standard growth conditions (F_{TMG} and F_{H2O} in Table 1), we obtained single-phase ε-Ga_2O_3 at 610 °C (sample D) or coexistence of the ε and β polymorphs at 650 °C (sample A). The latter film was mainly ε at the inlet and almost completely β at the outlet, whereas in the middle the two phases were mixed. Figure 2 shows XRD patterns of selected samples, taken respectively at inlet, center, and outlet position for different growth conditions. Peaks of the different phases can be clearly distinguished, namely, $2\theta = 59.87°$ for the (006) reflection of ε-Ga_2O_3 and $2\theta = 59.2°$ for the $(\bar{6}03)$ reflection of β-Ga_2O_3.[23,24] The larger full-width half-maximum of the peak associated with β-Ga_2O_3 may be caused by a lower crystalline quality of the material, a feature already reported for this polymorph in refs [18,19] where it was grown at temperatures below the optimal ones ($T \geq 700$ °C).

A gradual change of the epitaxial Ga_2O_3 polymorph, as observed by XRD in different positions of the substrate (Figure 2), has not been reported so far, regardless of the deposition technique. In ref 18, the two phases nucleated simultaneously on the substrate and they gave rise to microcrystalline epilayers but not to separated ε and β areas such as the ones presented in this work.

From the analysis of data reported in Table 1, it is evident how the β-Ga_2O_3 fraction increases when the growth rate decreases (i.e., lowering the supersaturation) for both growth temperatures. Moreover, from these data, it emerges that the transition from ε- to β-Ga_2O_3 occurs through a mixed-phase material for 650 °C, while at 610 °C the transition from one polymorph to the other is more abrupt. The change of the F_{H2O}/F_{TMG} ratio did not appear to have a substantial effect.

It is also noteworthy that a pure β phase film (or a large portion of it) was reproducibly obtained at 610 °C with a very low growth rate [i.e., GR ≤ 3 nm/min; see also Figure 2d]. Hence, by just reducing the TMG flow, it is possible to nucleate the β-phase also at 610 °C, which is in contrast to previous reports stating that β-Ga_2O_3 can be nucleated only at temperatures higher than 700 °C when utilizing H_2O and TMG as precursors.[14,15,25]

In Figure 3, we present a deposition temperature−growth rate phase diagram, in which the fraction of β-Ga_2O_3 of each sample is indicated as a color symbol and areas of pure β-Ga_2O_3 (blue), pure ε-Ga_2O_3, (red) and mixed phase (green)

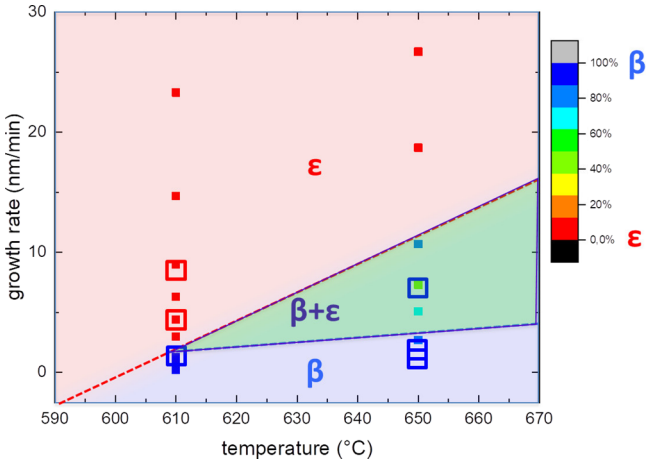

Figure 3. Phase diagram of β-Ga_2O_3 and ε-Ga_2O_3 as a function of growth rate (y axis) and deposition temperature (x axis). Colors of symbols correspond to the percentage of β-Ga_2O_3 obtained by XRD analysis, as indicated by the color bar on the right. Large open squares indicate samples grown with an F_{H2O}/F_{TMG} ratio of 1000.

https://doi.org/10.1021/acs.cgd.1c00863
Cryst. Growth Des. 2021, 21, 6393−6401

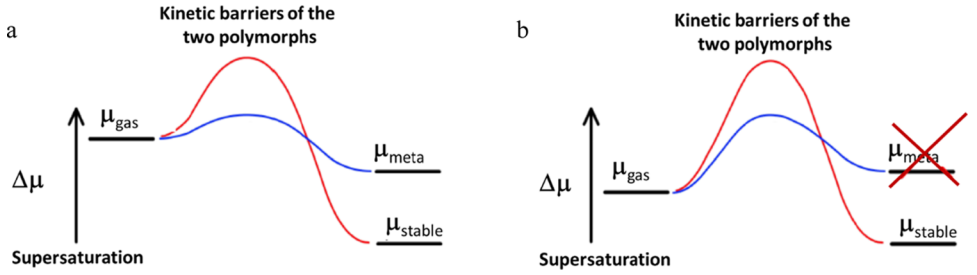

Figure 4. Schematic mechanism of the formation of metastable (a) or stable (b) phases depending on actual supersaturation $\Delta\mu = (\mu_{gas} - \mu_{meta})$ or $(\mu_{gas} - \mu_{stable})$; the kinetic nucleation barrier determines the nucleation probability of either polymorph at a given temperature (adapted from ref 40).

are highlighted. It is evident how pure β-Ga_2O_3 is achievable also at low temperature, provided that the growth rate (i.e., the supersaturation) is kept below a certain value. Moreover, the mixed phase region seems to be present only at 650 °C, while films grown at 610 °C are either predominantly β-Ga_2O_3 or ε-Ga_2O_3 depending on the GR.

Considering the literature on MOVPE deposition of β-Ga_2O_3, we identified the relevant growth parameters for this polymorph, keeping them as a reference for the assessment of the growth conditions applied in the present set of experiments. As discussed in the Experimental Section, the temperature of our substrate holder is homogeneous, which helps exclude the fact that the two Ga_2O_3 polymorphs observed in the same deposition run are due to a temperature gradient. Other possible effects to be considered for a physical explanation of our results are (i) the composition of the gas phase, (ii) the metastability of ε-Ga_2O_3 (that in principle could lead to solid−solid phase transition), and (iii) the role of gas phase supersaturation. In the following subsections, we will discuss them separately.

Influence of Oxygen Precursor Species. Previous works showed that β-Ga_2O_3 can be obtained at $T < 650$ °C by using O_2 instead of H_2O as an oxygen source.[26,27] Therefore, one could argue that in our case, the nucleation of β-Ga_2O_3 over ε-Ga_2O_3 could be attributed to chemical reactions that would convert, at least partially, H_2O into O_2; this is known as "oxygen evolution reaction" (OER). However, breaking the chemical bonds in the H_2O molecules requires a much larger energy than the thermal one provided in our reactor at the investigated growth temperatures. A literature analysis reveals that Ga_2O_3 nanoparticles—the Ga_2O_3 surface itself—could have a catalytic effect toward the production of O_2, so it is worthwhile to discuss if this could be a possible way to change the composition of the gas phase along our vertical MOVPE reactor. It has been theoretically suggested that α-[28] and β-Ga_2O_3[29] surfaces could have a catalytic effect on water, promoting the OER, but the process would require the application of an additional voltage in order to overcome the energetic barrier of the water splitting reaction. Also, the presence of a metal catalyst on the Ga_2O_3 surface, coupled to UV light irradiation, can actually promote the water splitting reaction.[30] In another article, the influence of oxygen vacancies in β-Ga_2O_3 on OER is suggested, but the authors state that a clear relationship is not yet demonstrated.[31]

Considering the available information and the results reported in literature, the possibility of a catalytic activity of ε-Ga_2O_3 surfaces to generate O_2 from H_2O seems extremely unlikely in our case, and we tend to exclude the presence of free O_2 as a promoter of nucleation of β-Ga_2O_3.

Solid−Solid $\varepsilon \rightarrow \beta$ Phase Transitions. It is known that ε-Ga_2O_3 is metastable and can convert to β-Ga_2O_3. However, the phase transformation occurs at temperatures higher than 900 °C, although the first mild signs of phase modification can be detected at 700 °C.[32] Furthermore, after solid−solid phase transformation, the converted β-Ga_2O_3 material is made of randomly oriented grains (i.e., no preserved epitaxial relation with the substrate).[32−34]

Considering that the growth temperatures of our substrate holder are set at 610 or 650 °C for the entire duration of the growth, we exclude that the cause for the presence of the β-Ga_2O_3 phase could be related to a thermally triggered phase conversion of a nucleated ε-Ga_2O_3 layer during the process. Moreover, the β-Ga_2O_3 observed in our films nucleates directly in this phase: this is supported by the collected XRD measurements, which evidences the sole $(\bar{2}01)$ orientation normal to the substrate (see Figure S5), while post-crystallization would most likely result in randomly oriented polygrains.

Kinetics and Thermodynamics Interplay: The Role of Supersaturation. As already discussed, the influence of a single parameter cannot explain the coexistence of ε- and β-Ga_2O_3 in the same film. However, this result can be explained considering that the local supersaturation along the horizontal reactor may vary considerably because of the gradual consumption of reactants, resulting in a concentration gradient in the gas phase (i.e., from the inlet toward the outlet). The measurable macroscopic effect of the variable supersaturation is the thickness gradient, that is, the GR variation. As reported in Table 1, the growth rate can be up to three times higher at the inlet side, where the precursors have the maximum concentration, with respect to the outlet side, where the precursors are impoverished. Of course, this also means that at the inlet, for a given substrate temperature, the supersaturation grants strongly off-equilibrium conditions while, at the opposite side, the thermodynamic conditions are closer to the equilibrium and sufficient to nucleate the stable β phase rather than the metastable one. This behavior, however, should not be seen as anomalous in view of Ostwald's step rule:[35] this rule was empirically derived from observations of solution and melt-grown crystals, and it states that crystallization from a disordered nutrient phase usually starts from the least stable polymorph. There are many experimental data that corroborate Ostwald's rule, for example, the early crystallization of anatase titanium dioxide from solutions or solid−solid crystallization starting from amorphous thin films, despite being metastable, with respect to the stable rutile phase.[36−38]

However, later reports showed how Ostwald's rule provided a correct description of polymorphism phenomenology, and

https://doi.org/10.1021/acs.cgd.1c00863
Cryst. Growth Des. 2021, 21, 6393−6401

that statistical thermodynamics, kinetics, and atomistic phenomena have to be considered to justify the nucleation and stabilization of metastable phases in the observed sequence.[39] In other words, Ostwald's step rule is always valid if a kinetic nucleation barrier, typical of each polymorph, is considered. The nucleation barrier ultimately expresses the probability of forming nuclei of one or the other phase depending on the relevant surface and substrate/film interface energy. A higher barrier implies low probability and vice versa. The kinetic nucleation barrier is specific to the surface energy of the outer crystallographic planes of a nucleus, including its rim, and the film/substrate interface, as recently pointed out by Meister.[40]

A question that immediately arises is this: if the supersaturation at the inlet side is so high that nucleation of the metastable phase becomes possible, why is the nucleation of the stable one prevented? A qualitative but useful explanation is provided in Figure 4, where we reported the chemical potentials of the supersaturated gas phase and of the solid stable or metastable Ga_2O_3. The use of chemical potential in Figure 4 should be considered an approximation, as it refers to individual particles leaving or joining a given phase; however, it provides a useful visual picture of the interplay of thermodynamics (chemical potential; change of free energy between starting and final system as the driving force of crystallization) and kinetics (density of surface sites; mobility of adsorbed species) in deciding what polymorph will be nucleated and grown. In the case of Ga_2O_3 deposition from the vapor phase, it is reasonable to assume that the schematic shown in Figure 4 applies to the minority component Ga.

In this framework, it is possible to give a semi-quantitative interpretation of the data presented in Table 1: at the inlet, the supersaturation $\Delta\mu$ is high and positive with respect to both polymorphs; however, the nucleation of the metastable one is favored by a lower activation barrier, as long as the process temperature is low (Figure 4a). If the epitaxial deposition takes place at higher temperatures (≥700 °C), the probability of overcoming the barrier of the stable phase increases so that the nucleation and stabilization of β phase is favored by the higher difference of Gibbs free energy. Such a situation is well documented by several works that show how β-Ga_2O_3 forms by MOVPE with H_2O and TMG at temperatures higher than 700 °C.[14,15,25]

Figure 4b refers to the case of the β phase grown at temperatures considerably lower than 700 °C by strongly decreasing the supersaturation (e.g., samples F and G).

It is interesting to observe that by just reducing the TMG flow, it is possible to nucleate and stabilize the β phase even at 610 °C (sample G). To the best of our knowledge, this is the first evidence of a single-phase β-Ga_2O_3 grown at such low temperatures using TMG and water as precursors. The presented experiments nicely show that the thermodynamic–kinetic interplay is decisive for the selection of the emerging Ga_2O_3 phase.

Our β-Ga_2O_3 samples are $(\bar{2}01)$-oriented, while ε-Ga_2O_3 samples are (001)-oriented (see Figure S6). For these phases and crystallographic orientations, it would therefore seem that when the level of supersaturation is sufficient to grow both polymorphs (see $\Delta\mu$ in Figure 4a), the nucleation of metastable (001) ε-Ga_2O_3 is favored.

To explain these experimental observations, we have to consider the classical nucleation theory[41,42] and the probability J of nucleation of islands on the heterosubstrate:

$$J = Z \exp\left(\frac{-\Delta G^*}{kT}\right) \tag{1}$$

where ΔG^* represents, for a given supersaturation, the work necessary to build up a nucleus of critical size, that is, the change of free energy obtained by summing the stabilizing (negative) internal energy and the destabilizing (positive) surface energy of the critical nucleus. The pre-exponential factor Z is the so-called Zeldovich factor, well known from the classical nucleation theory,[41,42] which expresses the probability that a nucleus will expand rather than dissolve. It depends on the work necessary to build up a cluster with a certain geometry (e.g., 2D disk and 3D dome), critical nucleus size, expressed as the number of elementary building blocks n^*, and temperature according to

$$Z = \sqrt{\frac{\Delta G^*}{3\pi kTn^{*2}}} \tag{2}$$

We deposited Ga_2O_3 on c-plane α-Al_2O_3, which implies a certain mismatch between the substrate and both Ga_2O_3 polymorphs, and consequently, the probable nucleation of 3D clusters rather than coherent 2D islands. Furthermore, it is likely that in the very first stages of nucleation, the elastic strain also plays a role, although very difficult to quantify due to the formation of rotational domains in the films for both phases.[12,43]

Let us consider the general expression of ΔG for a 3D nucleus of n atoms on a foreign substrate,[41,42]

$$\Delta G = n\Delta\mu + an^{2/3}\gamma_{\text{eff}} \tag{3}$$

where a represents the average surface associated to each external cluster's atom (building unit) and γ_{eff} is the effective specific surface energy that accounts for the γ_{vn}, γ_{sn}, γ_{vs} contributions, that is, the surface energies at the vapor–nucleus, substrate–nucleus and vapor–substrate interfaces, respectively. By differentiating eq 3 and putting it to zero, one can obtain the critical size n^* and critical free energy threshold ΔG^*:

$$n^* = \frac{Fa^3\gamma_{\text{eff}}^{\ 3}}{\Delta\mu^3} \qquad \Delta G^* = \frac{Fa^3\gamma_{\text{eff}}^{\ 3}}{\Delta\mu^2} \tag{4}$$

where F is a factor that changes with the nucleus shape. It is important to note that the critical nucleus size and formation work are strongly dependent on the supersaturation and specific effective surface energy. With this information, let us establish all terms of eq 1

$$J = \sqrt{\frac{\Delta\mu}{3\pi kT}} \exp\left(-\frac{Fa^3\gamma_{\text{eff}}^{\ 3}}{kT(\Delta\mu)^2}\right) \tag{5}$$

It must be noted that specific surface energy and supersaturation appear at powers 3 and 2, respectively, and consequently play a dominant role in setting the value of J. Therefore, in a first approximation, the geometrical factor F (shape of the nucleus) and a will be taken as independent of the crystallographic phase. This is acceptable even if the packing of O atoms and Ga tetrahedra and octahedra is rather different along the (001) and $(\bar{2}01)$ growth directions of ε and β epilayers, respectively. The surface energy is particularly important, as it appears to the third power within the exponential in the nucleation frequency expression, but $\Delta\mu$ is also important as it appears to the second power at the

https://doi.org/10.1021/acs.cgd.1c00863
Cryst. Growth Des. 2021, 21, 6393–6401

denominator of the negative exponential and as a multiplier under square-root in the pre-exponential term.

Therefore, for the case of Figure 4a [the chemical potential of the vapor phase $\mu_{gas} > \mu_{meta}, \mu_{stable}$; $\Delta\mu_{meta} = (\mu_{gas} - \mu_{meta}) < \Delta\mu_{stable} = (\mu_{gas} - \mu_{stable})$], if the effective surface energy were equal for the two polymorphs, the $(\bar{2}01)$-oriented β film would have the highest nucleation probability J, which however contradicts the experimental observations. To reconcile classical nucleation theory and experimental results, one must postulate that the monoclinic β-Ga_2O_3 clusters possess a higher surface energy than the clusters of orthorhombic ε-Ga_2O_3, so that the formation of the former is hindered. In the hypothesis of a typical layer-by-layer deposition, following 2D nucleation, one could conclude that the surface energy of $(\bar{2}01)$ β planes is higher than that of (001) ε planes; but this conclusion at the present state of knowledge would be speculative, especially for the first-to-grow nuclei on the sapphire. There are indeed hints that, at the first stage, the growth proceeds via 3D nucleation, island formation, and island coalescence to form a compact layer;[13] therefore, there might be considerable contributions to global nucleus energy also from the irregular sides of the islands, that is, other surfaces rather than solely $(\bar{2}01)$ ones. It is thus preferable to speak of "effective surface energy" of the nucleus. Figure 5a shows a relatively smooth surface for the ε-Ga_2O_3, except for the presence of a bunch of regular hexagonal platelets of typical size in the micron range, while at the outlet side part (Figure 5b), the β-Ga_2O_3 portion of film is essentially made of tiny islands with typical size (width and height) of some tens of nm.

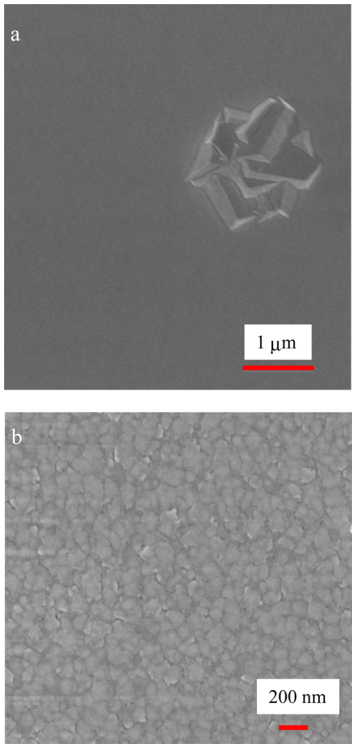

Figure 5. SEM images of sample *E* in the inlet (a—pure ε) and outlet (b—pure β) part of the substrate. The feature seen in (a) is included to focus the image of the otherwise featureless surface and is attributed to the expansion of a seed formed in the gas phase and fallen on the substrate. The 120° angles of the platelets are typical of the orthorhombic phase.

Clearly, these examples show how both effective surface energies and extension of subsequent clusters, along with kinetics, will substantially dictate the growth evolution after the thermodynamic–kinetic driven nucleation shown in Figure 4 and eq 5.

With this theoretical background, it is now possible to critically examine the series of experiments in Table 1 and make some meaningful comparisons:

i) Films A and D were grown with standard precursor flows at temperatures of 650 and 610 °C, respectively. The second one is completely ε because the growth temperature was too low to enable the nucleation of β phase (Figure 4a) even at the outlet side where the GR clearly indicates a strong decrease of supersaturation. The drop of supersaturation was, however, not sufficient to reach the conditions depicted in Figure 4b.

ii) Films A, B, and C were all grown at 650 °C but with variable TMG flow. The GR was obviously lower for lower TMG supply, so that we encounter now the conditions depicted in Figure 4b, not only at the outlet side but over a large fraction of the substrate. As a result, the β phase extended considerably up to the inlet side.

iii) Films D, E, F, and G were all grown at 610 °C, but the TMG flow ranged from standard, low, and very low. The films grown with TMG flow at the highest or lowest extreme were entirely ε or entirely β. The GR indicated an extremely low supersaturation for the β sample G. As discussed previously, this case is described in Figure 4b. The difference $(\mu_{gas} - \mu_{stable})$ must be weakly positive, while $(\mu_{gas} - \mu_{meta})$ is either nil or negative, so that it becomes possible to deposit the stable β polymorph, although at a very reduced GR. At such extremely low supersaturation, the island nucleation rate on the surface of the β film is actually so low that at the outlet side of layer G, we observed separated islands instead of a continuous and compact layer, as seen in the SEM picture in Figure 6. At the

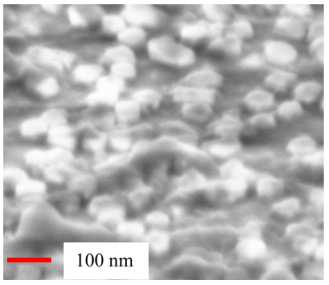

Figure 6. SEM image of a β-Ga_2O_3 sample grown at 610 °C with very low precursor supersaturation (G, outlet). The image was obtained by tilting the sample by 60°.

inlet side, the supersaturation was anyway sufficient to produce a thin but compact single-phase β film. Nonetheless, as previously discussed, for intermediate TMG flows β and ε polymorphs coexisted on the same slice.

iv) On the outlet side (Figure 4b), with the only exception of sample D (i.e., standard fluxes and lower substrate temperature of 610 °C), due to the drop of the precursor concentration along the gas flow direction, the chemical potential of the nutrient phase is so low that the supersaturation is hardly sufficient to provide the driving force for crystallization of β-Ga_2O_3 but insufficient for nucleation of ε-Ga_2O_3; hence, β becomes the only phase possible.

v) As a final case, let us consider the high-temperature growth of β-Ga_2O_3 films ($T \geq 700$ °C, not experimentally

https://doi.org/10.1021/acs.cgd.1c00863
Cryst. Growth Des. 2021, 21, 6393–6401

investigated in this work). Irrespective of the supersaturation, the films are invariably of the stable phase β because the temperature is high enough to provide a relatively high probability of overcoming the kinetic nucleation barrier (Figure 4a). Therefore, independent of surface energy, the nucleation of the β phase is favored because it allows the maximum gain of free energy. Furthermore, at the atomistic level, the higher temperature increases the surface mobility of adatoms, thus leading to the quick enlargement of nuclei and the achievement of flat surfaces.

CONCLUSIONS

In this work, we have presented a study of the effect of supersaturation, estimated from the growth rate, on the stabilization of ε-Ga_2O_3 and β-Ga_2O_3 grown by MOVPE on c-plane sapphire. In the analyzed films, the growth rate ranged between 0.2 and 25 nm/min, at temperatures of 650 and 610 °C, which allowed us to explore a wide range of supersaturation regimes.

Due to the decrease of precursor partial pressure along the flow direction, the deposition was faster at the inlet side and much slower at the outlet side of the reactor chamber, with a consequent thickness gradient along the substrate. The faster-grown portion of the film was ε while, at the slower-grown side, it was β. The ratio between β-Ga_2O_3 and ε-Ga_2O_3 areas could be modified by changing the reactant flows. In particular, a reduction of the TMG flow led to the extension of the β fraction until the film was entirely β even at growth temperatures as low as 610 °C. Contrarily to what was commonly reported in the literature, it is thus possible to obtain pure β-Ga_2O_3 films at temperatures lower than 700 °C, with TMG and water as precursors, provided that supersaturation is sufficiently low.

These results were interpreted in the framework of classical nucleation theory and Ostwald's step rule, considering the interplay of thermodynamic effects (supersaturation and different chemical potentials for the metastable ε phase and the stable β phase) and kinetic effects (related to different nucleation barriers for various crystallographic phases/planes).

The present results contribute to the understanding of the physical reasons ruling the stabilization of different Ga_2O_3 polymorphs, and they allow for the improvement of design and growth of this emerging wide band gap semiconductor.

ASSOCIATED CONTENT

Supporting Information

The Supporting Information is available free of charge at https://pubs.acs.org/doi/10.1021/acs.cgd.1c00863.

Reactor models and COMSOL Multiphysics simulations, details of the thickness measurements with optical reflectance and SEM images, and XRD measurements for pure-phase epitaxial films (PDF)

AUTHOR INFORMATION

Corresponding Authors

Matteo Bosi − *IMEM-CNR, Parma 43124, Italy;* orcid.org/0000-0001-8992-0249; Email: matteo.bosi@imem.cnr.it

Luca Seravalli − *IMEM-CNR, Parma 43124, Italy;* orcid.org/0000-0003-2784-1785; Email: luca.seravalli@imem.cnr.it

Authors

Piero Mazzolini − *Department of Mathematical, Physical and Computer Sciences, University of Parma, Parma 43124, Italy; IMEM-CNR, Parma 43124, Italy;* orcid.org/0000-0003-2092-5265

Francesco Mezzadri − *Department of Chemistry, Life Sciences and Environmental Sustainability, University of Parma, Parma 43124, Italy; IMEM-CNR, Parma 43124, Italy;* orcid.org/0000-0001-9505-1457

Roberto Fornari − *Department of Mathematical, Physical and Computer Sciences, University of Parma, Parma 43124, Italy; IMEM-CNR, Parma 43124, Italy*

Complete contact information is available at: https://pubs.acs.org/10.1021/acs.cgd.1c00863

Author Contributions

The manuscript was written through contributions of all authors. All authors have given approval to the final version of the manuscript. M.B. and L.S. contributed equally to this paper.

Notes

The authors declare no competing financial interest.

ACKNOWLEDGMENTS

Authors would like to acknowledge the work of Dr. Francesco Boschi for the design and modeling of the growth chamber used for the experiments of this paper. Dr. Peter Petrik (MFA—Institute for Technical Physics and Materials Science, Budapest, Hungary) is acknowledged for the ellipsometry measurements and the calculation of the refractive index of ε-Ga_2O_3. This work has benefited from the equipment and framework of the COMP-HUB Initiative, funded by the 'Departments of Excellence' program of the Italian Ministry for Education, University and Research (MIUR, 2018−2022) and by the program "Infrastructures" of the University of Parma.

REFERENCES

(1) *Gallium Oxide, Technology, Devices, Applications*; Pearton, S., Ren, F., Mastro, M., Eds.; Elsevier, 2018.

(2) Mastro, M. A.; Kuramata, A.; Calkins, J.; Kim, J.; Ren, F.; Pearton, S. J. Perspective—Opportunities and Future Directions for Ga2O3. *ECS J. Solid State Sci. Technol.* **2017**, *6*, P356−P359.

(3) Pearton, S. J.; Ren, F.; Tadjer, M.; Kim, J. Perspective: Ga2O3 for Ultra-High Power Rectifiers and MOSFETS. *J. Appl. Phys.* **2018**, *124*, No. 220901.

(4) Roy, R.; Hill, V. G.; Osborn, E. F. Polymorphism of Ga2O3 and the System Ga2O3-H2O. *J. Am. Chem. Soc.* **1952**, *74*, 719−722.

(5) Baldini, M.; Galazka, Z.; Wagner, G. Recent Progress in the Growth of β-Ga2O3 for Power Electronics Applications. *Mater. Sci. Semicond. Process.* **2018**, *78*, 132−146.

(6) Budde, M.; Splith, D.; Mazzolini, P.; Tahraoui, A.; Feldl, J.; Ramsteiner, M.; von Wenckstern, H.; Grundmann, M.; Bierwagen, O. SnO/β -Ga $_2$ O $_3$ Vertical *Pn* Heterojunction Diodes. *Appl. Phys. Lett.* **2020**, *117*, No. 252106.

(7) Bosi, M.; Mazzolini, P.; Seravalli, L.; Fornari, R. Ga2O3 Polymorphs: Tailoring the Epitaxial Growth Conditions. *J. Mater. Chem. C* **2020**, *8*, 10975−10992.

(8) Hou, X.; Zou, Y.; Ding, M.; Qin, Y.; Zhang, Z.; Ma, X.; Tan, P.; Yu, S.; Zhou, X.; Zhao, X.; Xu, G.; Sun, H.; Long, S. Review of Polymorphous Ga2O3 Materials and Their Solar-Blind Photodetector Applications. *J. Phys. D: Appl. Phys.* **2021**, *54*, No. 043001.

(9) Mezzadri, F.; Calestani, G.; Boschi, F.; Delmonte, D.; Bosi, M.; Fornari, R. Crystal Structure and Ferroelectric Properties of ε-Ga2O3 Films Grown on (0001)-Sapphire. *Inorg. Chem.* **2016**, *55*, 12079−12084.

(10) Ranga, P.; Cho, S. B.; Mishra, R.; Krishnamoorthy, S. Highly Tunable, Polarization-Engineered Two-Dimensional Electron Gas in ε -AlGaO $_3$/ε -Ga $_2$ O $_3$ Heterostructures. *Appl. Phys. Express* **2020**, *13*, No. 061009.
(11) Gottschalch, V.; Merker, S.; Blaurock, S.; Kneiß, M.; Teschner, U.; Grundmann, M.; Krautscheid, H. Heteroepitaxial Growth of α-, β-, γ- and κ-Ga2O3 Phases by Metalorganic Vapor Phase Epitaxy. *J. Cryst. Growth* **2019**, *510*, 76−84.
(12) Cora, I.; Mezzadri, F.; Boschi, F.; Bosi, M.; Čaplovičová, M.; Calestani, G.; Dódony, I.; Pécz, B.; Fornari, R. The Real Structure of ε-Ga2O3 and Its Relation to κ-Phase. *CrystEngComm* **2017**, *19*, 1509−1516.
(13) Hassa, A.; Grundmann, M.; von Wenckstern, H. Progression of Group-III Sesquioxides: Epitaxy, Solubility and Desorption. *J. Phys. D: Appl. Phys.* **2021**, *54*, No. 223001.
(14) Boschi, F.; Bosi, M.; Berzina, T.; Buffagni, E.; Ferrari, C.; Fornari, R. Hetero-Epitaxy of ε-Ga2O3 Layers by MOCVD and ALD. *J. Cryst. Growth* **2016**, *443*, 25−30.
(15) Schewski, R.; Wagner, G.; Baldini, M.; Gogova, D.; Galazka, Z.; Schulz, T.; Remmele, T.; Markurt, T.; von Wenckstern, H.; Grundmann, M.; Bierwagen, O.; Vogt, P.; Albrecht, M. Epitaxial Stabilization of Pseudomorphic α-Ga2O3 on Sapphire (0001). *Appl. Phys. Express* **2015**, *8*, No. 011101.
(16) Baldini, M.; Gogova, D.; Irmscher, K.; Schmidbauer, M.; Wagner, G.; Fornari, R. Heteroepitaxy of Ga2(1-x)In2xO3 Layers by MOVPE with Two Different Oxygen Sources. *Cryst. Res. Technol.* **2014**, *49*, 552−557.
(17) Park, S. H.; Lee, H. S.; Ahn, H. S.; Yang, M. Crystal Phase Control of ε-Ga2O3 Fabricated Using by Metal-Organic Chemical Vapor Deposition. *J. Korean Phys. Soc.* **2019**, *74*, 502−507.
(18) Zhuo, Y.; Chen, Z.; Tu, W.; Ma, X.; Pei, Y.; Wang, G. β-Ga2O3 versus ε-Ga2O3: Control of the Crystal Phase Composition of Gallium Oxide Thin Film Prepared by Metal-Organic Chemical Vapor Deposition. *Appl. Surf. Sci.* **2017**, *420*, 802−807.
(19) Chen, Y.; Xia, X.; Liang, H.; Abbas, Q.; Liu, Y.; Du, G. Growth Pressure Controlled Nucleation Epitaxy of Pure Phase ϵ- And β-Ga2O3 Films on Al2O3 via Metal-Organic Chemical Vapor Deposition. *Cryst. Growth Des.* **2018**, *18*, 1147−1154.
(20) Toby, B. H.; Von Dreele, R. B. GSAS-II: The Genesis of a Modern Open-Source All Purpose Crystallography Software Package. *J. Appl. Crystallogr.* **2013**, *46*, 544.
(21) Boschi, F. *PhD Thesis: Growth and Investigation of Different Gallium Oxide Polymorphs*; University of Parma, 2016.
(22) Pavesi, M.; Fabbri, F.; Boschi, F.; Piacentini, G.; Baraldi, A.; Bosi, M.; Gombia, E.; Parisini, A.; Fornari, R. ε-Ga2O3epilayers as a Material for Solar-Blind UV Photodetectors. *Mater. Chem. Phys.* **2018**, *205*, 502−507.
(23) Oshima, Y.; Víllora, E. G.; Matsushita, Y.; Yamamoto, S.; Shimamura, K. Epitaxial Growth of Phase-Pure ε-Ga2O3 by Halide Vapor Phase Epitaxy. *J. Appl. Phys.* **2015**, *118*, No. 085301.
(24) Playford, H. Y.; Hannon, A. C.; Barney, E. R.; Walton, R. I. Structures of Uncharacterised Polymorphs of Gallium Oxide from Total Neutron Diffraction. *Chem. Eur. J.* **2013**, *19*, 2803−2813.
(25) Wagner, G.; Baldini, M.; Gogova, D.; Schmidbauer, M.; Schewski, R.; Albrecht, M.; Galazka, Z.; Klimm, D.; Fornari, R. Homoepitaxial Growth of β-Ga2O3 Layers by Metal-Organic Vapor Phase Epitaxy. *Phys. Status Solidi* **2014**, *211*, 27−33.
(26) Tadjer, M. J.; Mastro, M. A.; Mahadik, N. A.; Currie, M.; Wheeler, V. D.; Freitas, J. A.; Greenlee, J. D.; Hite, J. K.; Hobart, K. D.; Eddy, C. R.; Kub, F. J. Structural, Optical, and Electrical Characterization of Monoclinic β-Ga2O3 Grown by MOVPE on Sapphire Substrates. *J. Electron. Mater.* **2016**, *45*, 2031−2037.
(27) Yao, Y.; Okur, S.; Lyle, L. A. M. M.; Tompa, G. S.; Salagaj, T.; Sbrockey, N.; Davis, R. F.; Porter, L. M. Growth and Characterization of α -, β -, and ϵ -Phases of Ga2O3 Using MOCVD and HVPE Techniques. *Mater. Res. Lett.* **2018**, *6*, 268−275.
(28) Zhou, X.; Hensen, E. J. M.; van Santen, R. A.; Li, C. DFT Simulations of Water Adsorption and Activation on Low-Index α-Ga2O3 Surfaces. *Chem. Eur. J.* **2014**, *20*, 6915−6926.
(29) Anvari, R.; Spagnoli, D.; Parish, G.; Nener, B. Density Functional Theory Simulations of Water Adsorption and Activation on the (−201) β-Ga2O3 Surface. *Chem. Eur. J.* **2018**, *24*, 7445−7455.
(30) Wang, Y.; Zhuang, P.; Yue, H.; Dong, H.; Zhou, X. Unraveling the Mechanism of Photocatalytic Water Splitting in α-Ga2O3 Loaded with a Nickel Oxide Cocatalyst: A First-Principles Investigation. *J. Phys. Chem. C* **2019**, *123*, 8990−9000.
(31) Liu, T.; Feng, Z.; Li, Q.; Yang, J.; Li, C.; Dupuis, M. Role of Oxygen Vacancies on Oxygen Evolution Reaction Activity: β-Ga2O3 as a Case Study. *Chem. Mater.* **2018**, *30*, 7714−7726.
(32) Fornari, R.; Pavesi, M.; Montedoro, V.; Klimm, D.; Mezzadri, F.; Cora, I.; Pécz, B.; Boschi, F.; Parisini, A.; Baraldi, A.; Ferrari, C.; Gombia, E.; Bosi, M. Thermal Stability of ε-Ga2O3 Polymorph. *Acta Mater.* **2017**, *140*, 411−416.
(33) Cora, I.; Fogarassy, Z.; Fornari, R.; Bosi, M.; Rečnik, A.; Pécz, B. In Situ TEM Study of K→β and K→γ Phase Transformations in Ga2O3. *Acta Mater.* **2020**, *183*, 216−227.
(34) Liao, Y.; Jiao, S.; Li, S.; Wang, J.; Wang, D.; Gao, S.; Yu, Q.; Li, H. Effect of Deposition Pressure on the Structural and Optical Properties of Ga2O3 Films Obtained by Thermal Post-Crystallization. *CrystEngComm* **2018**, *20*, 133−139.
(35) Ostwald, W. Studien Über Die Bildung Und Umwandlung Fester Körper. 1. Abhandlung: Übersättigung Und Überkaltnug. *Z. Phys. Chem.* **1897**, *22U*, 289−330.
(36) Kinsinger, N. M.; Wong, A.; Li, D.; Villalobos, F.; Kisailus, D. Nucleation and Crystal Growth of Nanocrystalline Anatase and Rutile Phase TiO2 from a Water-Soluble Precursor. *Cryst. Growth Des.* **2010**, *10*, 5254−5261.
(37) Mazzolini, P.; Gondoni, P.; Russo, V.; Chrastina, D.; Casari, C. S.; Li Bassi, A. Tuning of Electrical and Optical Properties of Highly Conducting and Transparent Ta Doped TiO2 Polycrystalline Films. *J. Phys. Chem. C* **2015**, *119*, 6988−6997.
(38) Mazzolini, P.; Acartürk, T.; Chrastina, D.; Starke, U.; Casari, C. S.; Gregori, G.; Bassi, A. L. Controlling the Electrical Properties of Undoped and Ta-Doped TiO2 Polycrystalline Films via Ultra-Fast-Annealing Treatments. *Adv. Electron. Mater.* **2016**, *2*, No. 1500316.
(39) Cardew, P. T.; Davey, R. J. The Ostwald Ratio, Kinetic Phase Diagrams, and Polymorph Maps. *Cryst. Growth Des.* **2019**, *19*, 5798.
(40) Meister, P. *Ostwald's Step Rule: A Consequence of Growth Kinetics and Nano-Scale Energy Landscape*. 2021, EGU21−8176.
(41) Kashchiev, D. Stationary nucleation. In *Nucleation*, 1st Edition; Butterworth-Heinemann, 2000.
(42) Markov, I. V. *Crystal Growth for Beginners*; World Scientific Publishing Company, 2003.
(43) Rafique, S.; Han, L.; Neal, A. T.; Mou, S.; Boeckl, J.; Zhao, H. Towards High-Mobility Heteroepitaxial β-Ga2O3 on Sapphire − Dependence on The Substrate Off-Axis Angle. *Phys. Status Solidi Appl. Mater. Sci.* **2018**, *215*, No. 1700467.

https://doi.org/10.1021/acs.cgd.1c00863
Cryst. Growth Des. 2021, 21, 6393−6401